HTS-Tape Magnetic Bearing for Ultra High-Speed Turbo Motor

R. Oliveira, X. Zeng, Member, IEEE, X. Pei, Senior Member, IEEE, R. Burke

Abstract—This paper aims to design superconducting magnetic bearing using HTS tape for a ultra high-speed turbo motor operating up to 120 000 rpm. Despite being a recent technology compared to conventional magnetic bearings, HTS passive bearings have many interesting features, such as reduced dimensions, easy implementation and excellent dynamic response at high speed. The results of the finite element simulation are promising as the levitation forces and the stiffness of the superconductor bearing are compatible with the design requirements. The main contribution of this paper lies in the use of short-circuited HTS coils, unlike previous systems that used HTS bulk.

Index Terms—High-temperature superconductors, superconductor magnetic bearing, superconductor tape, high-speed superconducting system

I. Introduction

HIGH-SPEED systems require a shaft holding mechanism with low friction or non-contact. Magnetic bearings are excellent solutions for these systems. In recent decades, materials engineering discoveries have allowed the development of superconducting magnetic bearing (SMB). They are self-stabilised devices, suitable for high-speed operation with simplified cooling system [1]–[3]. They presents technically innovative and generally are built with high-temperature superconductors (HTS) bulk type material, therefore they are passive systems [4]–[6].

Early work shows that passive magnetic suspension is applicable to shafts and wheels up to about weight of 10 kg suspending a centrifugal rotor for 30 000 rpm and an optical device rotating with 40 mm in diameter [1]. Radial-type superconducting magnetic bearing with 300 mm in diameter, using YBCO bulk reach levitation force density around 11 N/cm^2 at 77 K and 17 N/cm^2 at sub-cooled of 67 K [7], [8]. The use of HTS tapes instead of HTS bulks leads to significant advantages [9]–[11].SMB in motor systems is a promising area and worthwhile investigation [12]–[14].

This paper focus on the design of the SMB using HTS tapes and will applied in high-speed motor. This system have a horizontal position with radial SMB, instead of vertical orientation and axial bearings. An important contribution to the superconductor field is the behavior of the second-generation HTS tapes under ultra-high angular velocity of magnetic field, since the previous systems operate at less than 10 000 rpm [15]–[17].

It is intended to present the development of this work, which consists of the following steps:

- Design: definition of the topology, operating parameters and qualitative analysis. This will help the manufacture of a testing platform for high-speed (120 000 rpm), low torque (4 Nm) and an electric drive system (electric motor and subsystems, control strategy and measurement). The SMB design will be developed on this stage, where the forces, topology, permanent magnets arrangement and HTS tape are defined.
- Simulation: the finite element method will be used to analyse of electromagnetic force capabilities of the HTS-tape bearings at high-speed using 2D simulation. 2D axisymmetric mode is used to evaluate the static levitation force. 2D model in xy plane is used to investigate the stiffness when the rotor is centring.

On the next steps it is intended to reach the technology readiness level (TRL) stage 6 [18].

II. Static Levitation of HTS tape

Magnetic stress approach is used to determine the behaviour of the levitation force in superconductors. The magnetic stress is dependent on the magnetic field density and the total magnetic field vector is written in terms of a normal component B_n and a tangential (surface) component B_t (1).

$$\boldsymbol{B} = B_n \boldsymbol{n} + B_t \boldsymbol{t} \tag{1}$$

The magnetic force on the surface element consists of three terms, a magnetic tension σ_m proportional to the normal component, a magnetic pressure p_m proportional to the tangential field component, and a magnetic shear τ_m [19] (Fig. 1), as shown:

$$\sigma_m = \frac{B_n^2}{2\mu_0}, \quad p_m = \frac{B_t^2}{2\mu_0}, \quad \tau_m = \frac{B_n B_t}{\mu_0}$$

The method to calculate the force between a permanent magnet (PM) and a superconductor (SC) can be described by (2).

(Corresponding author: Xianwu Zeng.)
Roberto Oliveira and Xiaoze Pei are with the Dept. of Electronics Electrical Engineering, University of Bath, Bath, BA2 7AY, United Kingdom.
Xianwu Zeng and Richard Burke are with the Dept. of Mechanical Engineering, University of Bath, Bath, BA2 7AY, United Kingdom (e-mail: xz2478@bath.ac.uk).

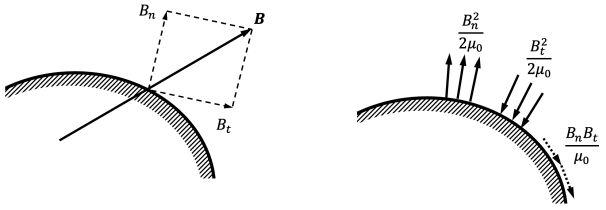

Fig. 1. Normal and tangential components of the magnetic field vector at a surface and the corresponding magnetic stresses.

$$F = \frac{1}{2\mu_0}\int[(B_n^2 - B_t^2)\boldsymbol{n} + 2B_nB_t\boldsymbol{t}]dA \qquad (2)$$

where $\boldsymbol{n}$ is the outward normal from body (radial component) and $\boldsymbol{t}$ is the tangential (axial component) of the magnetic induction. This equation presents the total force on the magnetic sources in the body [19].

The analysis can be made for the static levitation of type II superconductors which presents repulsive (due to diamagnetism) and attractive (due to magnetic flux pinning) forces. From the application of the Maxwell stress tensor on the surface of the superconductor in the presence of an external field, the magnetic force normal on the body can be expressed by (3)

$$F_n = \frac{1}{2\mu_0}\int(B_n^2 - B_t^2)dA \qquad (3)$$

Among the topological possibilities of a radial bearing, the axial magnetisation is very attractive topology. Axial magnetisation uses the magnets are axially magnetised and this configuration features flux concentrate in the radial direction.

SMB radial using outer configuration can be assembled with the HTS outside. This topology is called radial outer (Fig. 2). This configuration may allow variations in the type of shaft that may or may not have slots for the accommodation of the permanent magnets. The radial outer topology with axial magnetisation is chosen for high-speed motor system since it does not need a flux concentrator between the magnets and HTS tapes, allowing to construct a more compact magnetic bearing.

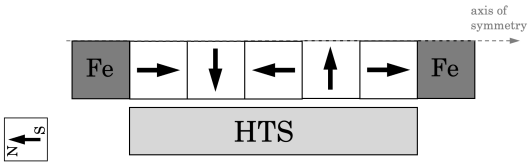

Fig. 2. Radial outer topology.

III. SMB Design

This superconducting bearing aims to stabilise a shaft for ultra-high speed motor application. Fig. 3 present the main geometric dimension of the shaft with radial SMB. PMs are mounted in Halbach array configuration and the size of each is determined by its thickness (a) and its diameter (b). Inserting the magnetic bearing at the ends of the rotor will change its weight. The bearing volume will depend on the geometry and the dimension of a, shown in Fig. 3, which is varied from a=5 mm (Topol-A), 7 mm (Topol-B) to 10 mm (Topol-C) with b held constant ($b = d_{outer}$). Table I presents the rotor volume and weight with a=10 mm.

Arnold Magnetic Technologies N52 permanent magnets are selected and the main parameters are B_r = 1.45 T, H_{cB} = 979 kA/m, H_{cJ} = 875 kA/m and BH_{max} = 406 kJ/m^3. Due to the high value of B_r and H_{cB}, the demagnetisation will depend on a the temperature rise and strong vibrations, which is not expected for this type of system.

The evaluated SMB considered two assemblies, the first configuration with 4 short-circuited HTS coils, 2 coils at each end of the shaft and the second configuration with 6 short-circuited HTS coils, 3 coils at each end. Different numbers of turns including 5, 10 and 17 were analysed. Details of the HTS tape is presents on Table II. The gap between PM and HTS coil is varied between 2 and 10 mm.

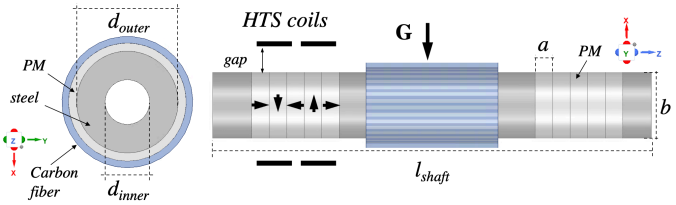

Fig. 3. Illustration of the shaft with SMB.

TABLE I
Volume and weight of the rotor with SMB and a=10 mm (Topol-C).

Volume	Steel 1010	NdFeB	Carbon fiber
cm^3	133.59	117.69	25.95
Density	Steel 1010	NdFeB	Carbon fiber
g/cm^3	7.87	7.6	1.6
Weigth	Steel 1010	NdFeB	Carbon fiber
kg	1.05	0.89	0.04
Total (kg)	1.98		
Total (N)	≈20.00		

TABLE II
Specifications of the superconductor

Description	Values
Manufacturer	Shanghai Superconductor
Conductor type	ST-12-L
Width [mm]	12
Thickness of HTS layer [μm]	2
Minimum I$_c$ @77 K [A]	500
I$_c$ of single tape @77 K [A]	510
I$_c$ of single tape @65 K [A]	1100
Resistance at 300 K [mΩ/m]	100

IV. Modelling

Two models are built for static and dynamic simulation. 2D z-axisymetric model is used to calculate the static force as a function of the gap, which is the interaction between the HTS coil and the set of permanent magnets (IV-A). In this evaluation, different dimensions are considered for each magnet of the array and HTS short-circuited coils with different number of turns.

The 2D xy-plane with 1D HTS representation model investigate the dynamic behaviour of the superconducting bearing (IV-B). The behaviour of the current in the coils and the forces due to the misalignment of the bearing are also calculated. This model is based on the study presented and developed by [20]–[22].

A. Static Force Modelling

Static force considers the calculation of the force due to weight, which is presented in (4).

$$\boldsymbol{P} = mg \tag{4}$$

The radial and axial force were obtained through an 2D z-axisymmetric model, according to Fig. 4. The magnetic force was calculated by integrating the vector presented in (5). Stiffness (k_z) describes the response of the magnetic force in front of changes in the position and velocity of the levitated body. According to (6) it is the negative of the derivative of the total magnetic force, in relation to the referred axial position.

$$\boldsymbol{F} = \boldsymbol{n} \cdot T = -\frac{1}{2}\boldsymbol{n}(\boldsymbol{H} \cdot \boldsymbol{B}) + (\boldsymbol{n} \cdot \boldsymbol{H})\boldsymbol{B}^T \tag{5}$$

$$k_z = -\left.\frac{\partial F}{\partial z}\right|_0 \tag{6}$$

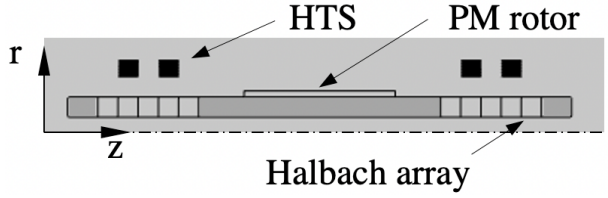

Fig. 4. Illustration of the shaft with SMB and 4 short-circuited HTS coils.

In this model, $\boldsymbol{H}$-formulation is used, which allows the calculation of the field of the permanent magnet, according to (7) and (8). The nonlinear resistivity of the superconductor is calculated by power law $\boldsymbol{E}$-$\boldsymbol{J}$ (9) in both static and dynamic models.

$$\boldsymbol{J} = \nabla \times \boldsymbol{H} \tag{7}$$

$$-\frac{\partial \boldsymbol{B}}{\partial t} = \nabla \times \boldsymbol{E} \tag{8}$$

$$\boldsymbol{E} = E_0 \left(\frac{|\boldsymbol{J}|}{J_c}\right)^n \frac{\boldsymbol{J}}{J_c} \tag{9}$$

The radial force (static force in the r-direction) is calculated by integrating the current density and magnetic field density. The electromagnetic stiffness is calculated based on the radial and axial magnetic field components, obtained from the finite element software, according to (5). Each step of 1 mm is used to move the HTS coils along the z-axis.

B. Dynamic Modelling

The dynamic 2D xy-plane model consideres the 1D superconducting tape method using a $\boldsymbol{T}$-$\boldsymbol{A}$-formulation, as shown in Fig. 5. The current density is calculated from the current vector potential ($\boldsymbol{T}$), (10), which considers the $\boldsymbol{A}$-formulation, (11), governing the domain external to the tape. Based on the model presented by [20], an initial value of $\boldsymbol{T}$=0.5 mA/m is applied on each HTS tape. It also considers that the tapes are in the presence of a magnetic field generated by permanent magnets whose direction of the rotating flux is described by $B_r \cos(2\pi f_r t)$ in the x-direction and $B_r \sin(2\pi f_r t)$ in the y-direction whose magnitude is 1.45 T and frequency f_r. The dynamics simulation is imposed by the movement of the magnetic field that emulates the speed of the rotor. This approach is useful to investigate the magnetic flux distribution.

$$\boldsymbol{J} = \nabla \times \boldsymbol{T} \tag{10}$$

$$\boldsymbol{B} = \nabla \times \boldsymbol{A} \tag{11}$$

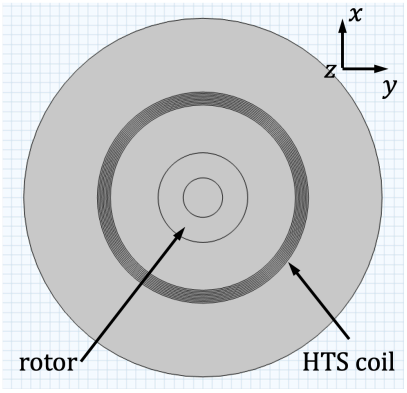

Fig. 5. Illustration of the model with a rotating flux.

V. Simulations Results

Fig. 6 shows the magnetic flux density in the Halbach array. This configuration has a pole pitch of 20 mm and enhances the magnetic field density, which is ≈0.6 T at 2 mm above the shaft, capable of meeting the initial system requirements.

The static force provided by the interaction of PM and HTS coils for different topologies of magnets and coils is shown in Fig. 7. The legend with index named A, B and C that represent the thickness of the PM (5, 7 and 10 mm, respectively), the number is related with the numbers of

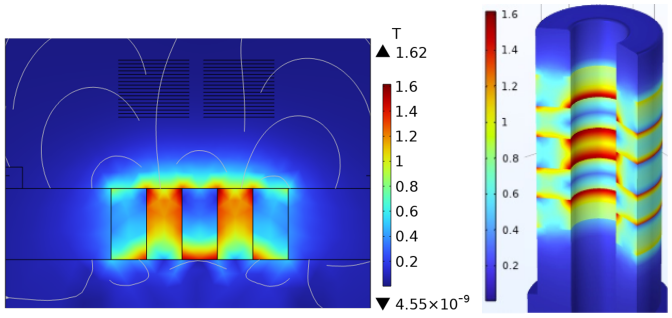

Fig. 6. Illustration of the shaft with PM. On left side a 2D model front view, and right side a revolution around z-axis.

turns of HTS coils (5, 10 and 17 turns) and the subscript is the total number of short-circuited HTS coils (4 or 6).

The gap variation has a strong impact on the force and this influence is presented quantitatively. Topol-C10$_4$, C17$_4$ or C17$_6$ configuration presents minimum conditions for bearing operation, with a holding force of approximately 60 N, 70 N and 90 N, respectively.

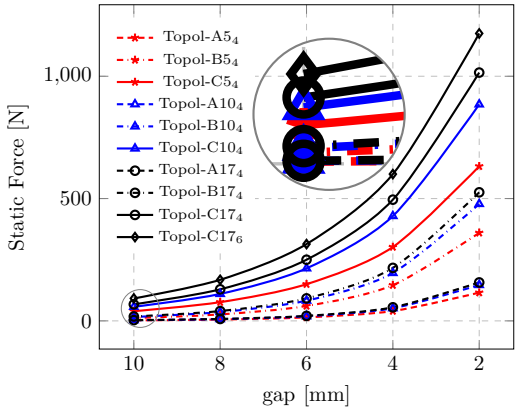

Fig. 7. Static force for different PM arrangement and gaps.

The relationship between the number of turns of each HTS coil with the static force is presented in Fig. 8 using Topol-C$_4$, which has 4 HTS short-circuited coils. The use of coils with more than 17 turns does not present any considerable increase in force.

The stiffness curves as a function of the gap variation of 5 and 10 mm for Topol-C17$_4$ and C17$_6$ are shown in Fig. 9. These values can be considered sufficient for this small rotor [23]–[25].

Magnetic flux density is presented in Fig. 10 with maximum of 0.7 T on the PM surface. In this computational model in xy plane, it is not possible to represent the Halbach configuration, so the maximum flux density is applied using the value obtained with the axysymmetric modeling (along z-axis) in the HTS coil region. The value of J/J$_c$ is approximately 0.7 as shown. Fig. 11 shows the current density in turn number 1, 5 and 10 in a quarter-section with arc length of 30 mm on the first turn. The winding is short-circuited and has the same circulating current.

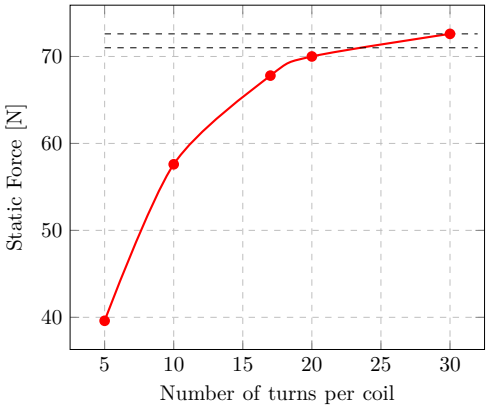

Fig. 8. Radial static force for different topologies with gap=10 mm.

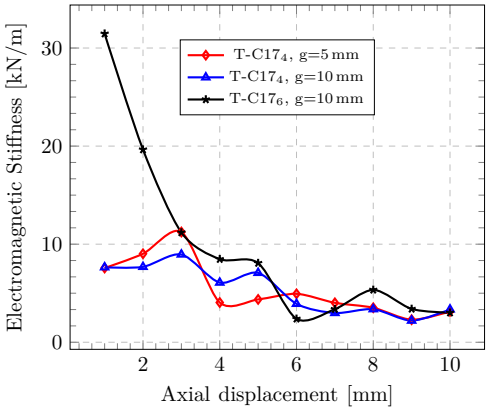

Fig. 9. Stiffness evaluated in the interaction region of the PM and HTS coil, considering 4 and 6 short-circuited HTS coils (17 turns each one) with a gap of 5 and 10 mm.

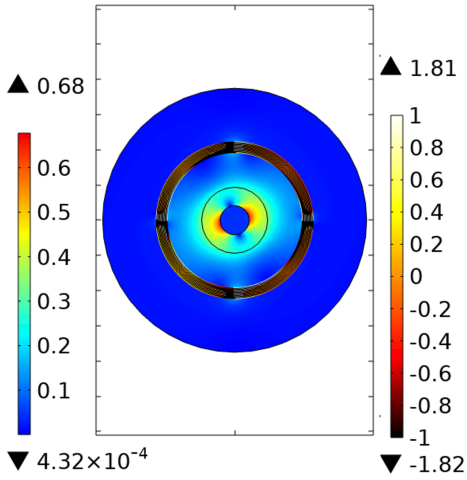

Fig. 10. Magnetic flux density (left legend [T]) and J/J$_c$ (right legend [-]) at 8 ms.

The SMB design with 10 turns of HTS coil using the magnetic flux density provided by Topol-C10 is presented in Fig. 12, The maximum flux density on HTS coil surface close to the PM increases by 23.6% and on the surface far from the PM decreases by 40.24% when the rotor is 2 mm

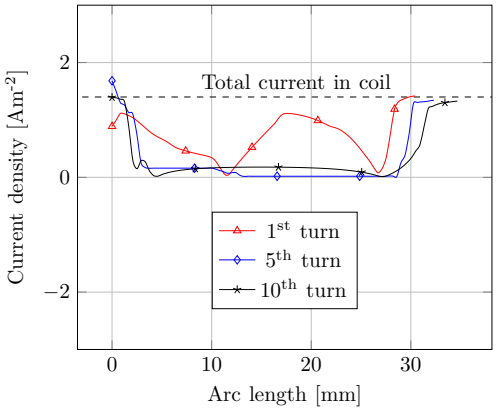

Fig. 11. Current density in different turns of short-circuited coil.

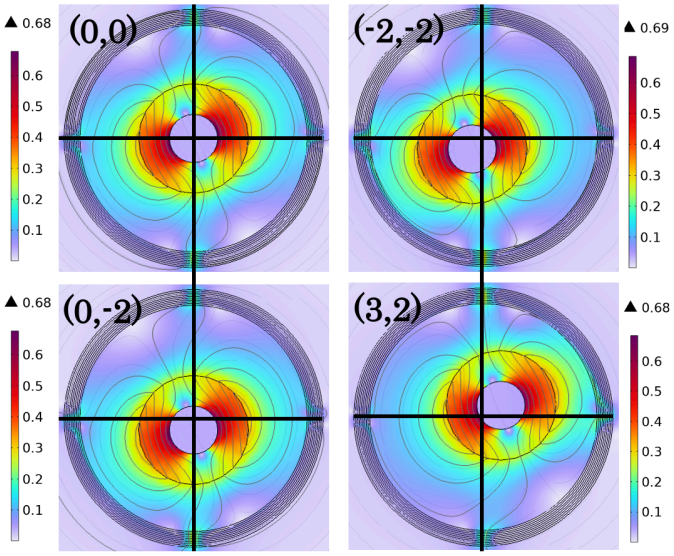

Fig. 12. Misalignment of HTS coil, where the Cartesian's coordinates showed is the displacement in millimetres, with (0,0) as the origin position.

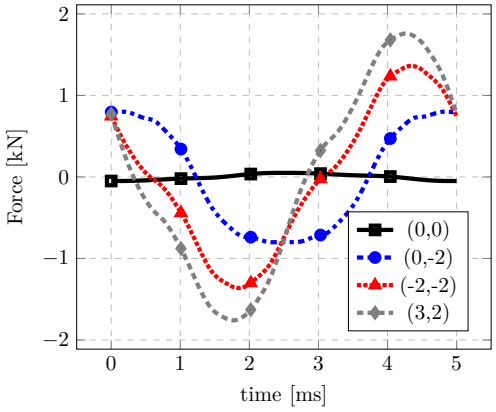

Fig. 13. Force provided by SMB when misalignment.

off-centre. Fig. 13 shows the force of SMB when there is a misalignment, which eventually can restore the shaft to the centre.

VI. Conclusions

The paper investigates superconducting magnetic bearing using HTS tape. It is in the preliminary design stage and focuses on qualitative analysis and numerical calculation of fundamental parameters. The simulation results shows that the superconducting magnetic bearing system can operate with a gap of 10 mm. Permanent magnets with 10 mm thickness with the number of tures of 10 and 17 for HTS coil is sufficient to keep the magnetic bearing operating.

Based on the static force results the use of a short-circuited HTS coils with 6 coils and 17 turns each significantly exceeds the requirements. The stiffness is higher, which makes this a preferable option.

The stiffness of SMB designed in this paper is sufficient to operate the rotor and keep it in a stable levitation position. The electromagnetic stiffness in the SMB is lower than the conventional magnetic bearing, however, this shaft is merged with the rotor of the motor and the magnetic rigidity would be increased by this interaction.

Dynamic simulation results indicate that the rotor can be supported by HTS coils. The amount of HTS coil is sufficient to keep the levitation steady and can restore the original position of the shaft when there is misalignment.

References

[1] F. Werfel, U. Flögel-Delor, R. Rothfeld, D. Wippich and T. Riedel, "Application advances in hts bearing technology," in Proc. 7th International Symposium on Magnetic Bearings, Zurich, Switzerland, 2000, pp. 23–25.

[2] M. Sparing, T. Espenhahn, G. Fuchs, M. Hossain, A. Abdkader, K. Nielsch, C. Cherif and R. Hühne, "Analysis of the high-speed rotary motion of a superconducting magnetic bearing during ring spinning," Engineering Research Express, vol. 2, no. 3, p. 035039, 2020.

[3] M. Hossain, M. Sparing, T. Espenhahn, A. Abdkader, C. Cherif, R. Hühne and K. Nielsch, "In situ measurement of the dynamic yarn path in a turbo ring spinning process based on the superconducting magnetic bearing twisting system," Textile Research Journal, vol. 90, no. 7-8, pp. 951–968, 2020.

[4] M. Strasik, J. Hull, J. Mittleider, J. Gonder, P. Johnson, K. McCrary and C. McIver, "An overview of boeing flywheel energy storage systems with high-temperature superconducting bearings," Superconductor science and technology, vol. 23, no. 3, p. 034021, 2010.

[5] F. Werfel, U. Flöegel-Delor, R. Rothfeld, T. Riedel, B. Goebel, D. Wippich and P. Schirrmeister, "Superconductor bearings, flywheels and transportation," Superconductor Science and Technology, vol. 25, no. 1, p. 014007, 2011.

[6] S. Klöppel, C. Muehsig, T. Funke, C. Haberstroh, U. Hesse, D. Lindackers, S. Zielke, P. Sass and R. Schoendube, "Superconducting bearings for a lhe transfer pump," in IOP Conference Series: Materials Science and Engineering, vol. 278, no. 1. IOP Publishing, p. 012029, 2017.

[7] N. Koshizuka, "R&D of superconducting bearing technologies for flywheel energy storage systems," Physica C: Superconductivity and its applications, vol. 445, pp. 1103–1108, 2006.

[8] X. Ren, M. Feng and T. Ren, "Design and optimization of a radial high-temperature superconducting magnetic bearing," IEEE Transactions on Applied Superconductivity, vol. 29, no. 2, pp. 1–5, 2018.

[9] E. Kurbatova, E. Kushchenko and P. Kurbatov, "Comparison of magnetic systems with hts bulks and hts tape for non-contact bearings," in 2020 21st International Symposium on Electrical Apparatus Technologies (SIELA). IEEE, pp. 1–4, 2020.

[10] M. Osipov, D. Abin, S. Pokrovskii, and I. Rudnev, "Investigation of hts tape stacks for levitation applications," IEEE Transactions on Applied Superconductivity, vol. 26, no. 4, pp. 1–1, 2016.
[11] F. G. R. Martins, F. Sass, A. C. Ferreira and R. de Andrade, "A novel magnetic bearing using rebco double crossed loop coils," IEEE Transactions on Applied Superconductivity, vol. 28, no. 4, pp. 1–5, 2018.
[12] T. Espenhahn, M. Sparing, A. Berger, K. Nielsch and R. Hühne, "Dependency of hysteretic loss on speed and tilt in a rotating superconducting magnetic bearing," Superconductor Science and Technology, vol. 34, no. 12, p. 125004, 2021.
[13] M. Minamitani, S. Takimura and S. Ohashi, "Design of the hts magnetic bearing rotor incorporated the secondary of the induction motor," in 2021 IEEE International Magnetic Conference (INTERMAG). IEEE, pp. 1–5, 2021.
[14] S. Siems, H. May, E. Portabella and W. Canders, "Application of htsc-bearings for high speed machines," in Proceedings of the 7th Int. Symposium on Magnetic Bearings, ETH-Zurich, Schweiz, pp. 607–612, 2000.
[15] A. K. Kameni, J. Leveque, B. Douine, S. Mezani and D. Netter, "Influence of speed variation of a transverse magnetic field on a magnetization of hts cylinder," IEEE Transactions on Applied Superconductivity, vol. 21, no. 4, pp. 3434–3441, 2011.
[16] G.-D. Nam, H.-J. Sung, C. Kim, J. Lee, R. A. Badcock, Z. Jiang and M. Park, "Design and performance analysis of a dynamo-type hts flux pump for a 10 kW superconducting generator," IEEE Transactions on Applied Superconductivity, vol. 30, no. 4, pp. 1–5, 2020.
[17] Z. Deng, W. Zhang, L. Kou, Y. Cheng, H. Huang, L. Wang, J. Chen, Z. Ke and Q. Ma, "An ultra-high-speed maglev test rig designed for hts pinning levitation and electrodynamic levitation," IEEE Transactions on Applied Superconductivity, vol. 31, no. 8, pp. 1–5, 2021.
[18] R. J. Terrile, F. G. Doumani, G. Y. Ho, and B. L. Jackson, "Calibrating the technology readiness level (trl) scale using nasa mission data," in 2015 IEEE aerospace conference. IEEE, pp. 1–9, 2015.
[19] F. C. Moon, Superconducting levitation: applications to bearings and magnetic transportation. John Wiley Sons, 2008.
[20] M. Ainslie, et al. "A new benchmark problem for electromagnetic modelling of superconductors: the high-T_c superconducting dynamo." Superconductor Science and Technology 33.10: 105009, 2020.
[21] G. Li, C. Li, Y. Xin, W. Hong,W. Li,T. Yang B. Li, "Dynamic modelling methodology for an HTS energy converter using moving mesh," Superconductor Science and Technology, 34(10), 105006, 2021.
[22] C. Li, G. Li, Y. Xin, B. Li, "Mechanism of a novel mechanically operated contactless HTS energy converter." Energy, 241, 122832, 2022.
[23] F. N. Werfel et al., "Impact of Cryogenics and Superconducting Components for HTS Magnetic Levitation Devices," in IEEE Transactions on Applied Superconductivity, vol. 27, no. 4, pp. 1-5, June 2017, Art no. 3600905.
[24] M. Komori and T. Hamasaki, "Improvement and evaluation of bearing stiffness in high Tc superconducting magnetic bearing," in IEEE Transactions on Applied Superconductivity, vol. 11, no. 1, pp. 1677-1680, March 2001.
[25] C. Jin, Y. Xu, J. Zhou. Active magnetic bearings stiffness and damping identification from frequency characteristics of control system. Shock and Vibration, 2016.